A General Approach for Optimal Design of Parallel Manipulators

Y.J. Lou, G.F. Liu, and Z.X. Li

Abstract— **This work intends to deal with the optimal kinematic synthesis problem of parallel manipulators. A unified framework is proposed for optimal design of parallel manipulators. By observation that regular (e.g., hyperrectangular) workspaces are desirable for most machines, we propose the concept of *effective regular workspace*, which reflects both requirements on the workspace shape and quality. Dexterity index is utilized to characterize the effectiveness of the workspace. Other performance indices, such as manipulability, stiffness, and minimal natural frequency, can be readily included. The optimal design problem is then formulated to find a manipulator geometry that maximizes the effective regular workspace. Since the optimal design problem is a constrained nonlinear optimization problem without explicit analytical expression, the controlled random search (CRS) technique, which was reported robust and reliable, is applied to numerically solve the problem. Some typical parallel manipulators, the five-bar parallel linkage, the 3-RRR planar parallel manipulator, the rotational DELTA robot, and the Stewart-Gough platform are employed as examples to demonstrated the design procedure.**

Index Terms— **optimal design, parallel manipulators, effective regular workspace, controlled random search, dexterity.**

I. Introduction

PARALLEL manipulators are widely accepted as ideal mechanisms for use in manufacturing industries for their superior properties over serial counterparts, such as low inertia, high stiffness, and high precision. However, relatively small workspace, complex input-output relationship, and abundance of singularities in their workspaces decline parts of above mentioned advantages. Choosing a set of geometric parameters so as to achieve desired/optimal performance is of vital significance in robotics research.

Among all kinematic measures, workspace is a basic yet most important index in design of a parallel manipulator. In regard to workspace requirements, there're two types of formulation of the design problem. One is to generate a manipulator whose workspace contains a prescribed workspace [1][2][3][4][5]. Gosselin and Guillot [6] presented an algorithm for the workspace optimization of planar manipulators, where the objective is to obtain a workspace that is as close as possible to a prescribed one. The other possible formulation is to find the geometry of a parallel manipulator that maximizes the workspace. A parallel manipulator designed only for maximum workspace may not however be a good design in practice. It's possible that the manipulator with maximum workspace has undesirable kinematic characteristics such as poor dexterity or manipulability. Stamper, Tsai, and Walsh [7] indicate this problem through an example of a 3-dof translational parallel manipulator.

In order to avoid the undesirable effects of workspace maximization, researchers introduced other performance criteria into the optimal design problem. Gosselin and Angeles designed a planar 3-DOF parallel manipulator [8] and a spherical 3-DOF parallel manipulator [9] by maximizing the workspace volume while taking into account the isotropy index. Pham and Chen [10] proposed to maximize the workspace of a parallel flexture mechanism subject to the constraints about a global measure and a uniformity measure of manipulability. In [7] Stamper et al. proposed to maximize the total volume of well-conditioned workspace. In the design problem, the objective function was chosen as the integral of inverse condition number of the kinematic Jacobian matrix over the workspace, and the link lengths of each subchain were normalized as a constraint. In addition to the workspace volume index, Stock and Miller [11] employed a linear combination of the manipulability and workspace indices in the objective function, where the coefficients are weights assigned to the two indices. The optimal design problem then becomes a mixed multi-criteria optimization problem.

In this paper, we propose a new optimization problem for design of parallel manipulators. The design objective is to maximize so called *effective regular workspace*. It is defined as a regular geometric object, e.g. a cube or a ball in 3-dimensional case, every point of which not only is contained in the manipulator workspace, but also possesses good dexterity. In practice a regular-shaped workspace with good dexterity is always desirable. It is well known that parallel manipulators often have irregular-shaped workspaces due to their complex kinematic structure. A design solely for maximal workspace may neither have maximal regular workspace, nor good dexterity over its workspace. In this paper, we choose to maximize the regular-shaped workspace while subject to the dexterity constraints. The optimal design problem is a multimodal constrained nonlinear optimization problem with no explicitly analytical expression. Gradient-based algorithms are not good enough in dealing with this problem since gradients and Hessians are not readily evaluated. we thus resort to a direct search method, the controlled random search (CRS) technique, which was remarked reliable and robust [12].

The paper is organized as follows. In section II, we formulate the optimization problem for design of parallel manipulators. In section III we present a basic CRS algorithm and provide an overall algorithm for solution of the optimization problem. In Section IV-VII, we use examples of a five-

This project is supported by RGC Grant No. HKUST 6187/01E, HKUST 6221/99E, and CRC98/01.EG02.

Y.J. Lou and Z.X. Li are both with the Dept. Electrical and Electronic Engineering, The Hong Kong University of Science and Technology, Clear Water Bay, Kowloon, Hong Kong SAR, China. (email: louyj@ust.hk; eezxli@ee.ust.hk)

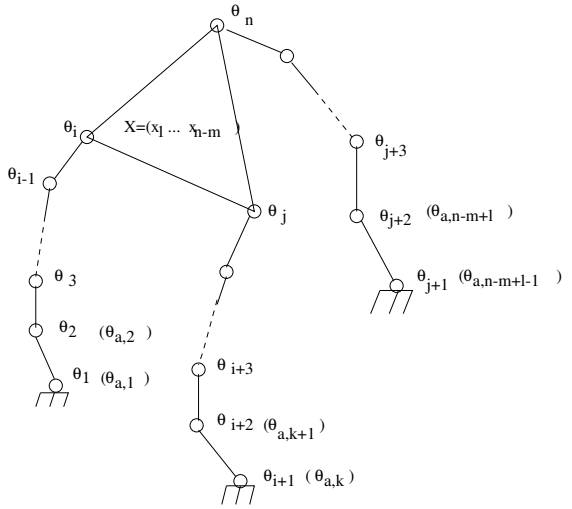

Fig. 1. Coordinate systems for a parallel manipulator

bar parallel linkage, a planar 3-RRR parallel manipulator, a rotational DELTA robot, and a 6-dof Stewart-Gough platform to indicate the design procedure and technique. We make Discussions and remarks on the the results and the design technique in section VIII and draw a conclusion in Section IX.

II. Formulation of the optimal design problem

A parallel manipulator, as shown in Fig. 1, consists of several open subchains connected in parallel to a common rigid body, known as the end-effector. The ambient space E of the manipulator is given by the Cartesian product of the joint spaces of all the joints that make up the manipulator. We denote by $\Theta \in \mathbb{R}^n$ the local coordinates of E. The loop closure equations of the manipulator are denoted by

$$H : E \longrightarrow \mathbb{R}^m, \Theta \longmapsto H(\Theta) = \begin{bmatrix} h_1(\Theta) \\ \vdots \\ h_m(\Theta) \end{bmatrix} = 0. \quad (1)$$

Note that the loop closure equations are obtained by equating pairwise the end-effector positions from each of the subchains. Let $\theta \in \mathbb{R}^{n-m}$, $\theta \subset \Theta$, be the set of joint variables of all actuators, i.e., the system is normally actuated, and $X \in \mathbb{R}^{n-m}$ the Cartesian coordinates representing the position and orientation of the end-effector. The inverse kinematics problem is to solve the corresponding θ from a given X using (1). We denote by ρ this inverse kinematics map.

$$\theta_i = \rho_i(X, \alpha), \quad i = 1, \cdots, n-m \quad (2)$$

where α is the set of kinematic parameters, e.g. the link lengths, the position of base points of each subchain, the relative arrangement of each axis, and the size and shape of the end-effector, etc. In practice, we may only focus on a subset of those parameters, known as design kinematic parameters (or design parameters for brevity) while fixing the remaining parameters due to some practical restrictions. Hereafter $\alpha \in \mathbb{R}^p$ denotes only the set of design parameters we're interested. Differentiating (1) yields its differential kinematics which can in general written as

$$\dot{\theta} = J\dot{X}, \quad (3)$$

where $J = J(X, \theta, \alpha)$ is the familiar kinematic Jacobian matrix for parallel manipulators, mapping Cartesian velocity $\dot{X}$ to joint rate $\dot{\theta}$.

A. The objective function

In manipulator design, a regular workspace (more specificly, a hyperrectangle) is usually provided as a design objective based on the types of manufacturing tasks and the working environment. This regular workspace is required to be contained in the workspace generated by the resultant manipulator such that it can conduct prescribed tasks. Maximization of the regular workspace among all possible designs is always desirable from the manufacturing perspects.

Let $W = W_1 \oplus W_2 \subset \mathbb{R}^6$ be a regular Cartesian workspace for a general parallel manipulator, where W_1 is the translational workspace while W_2 the rotational workspace. A measure for W can be derived based on that for W_1 and W_2. Assume that W_1 and W_2 are both rectangular parallelepipeds and l_i, w_i, h_i, $i = 1, 2$, the lengths of three independent edges. The size of regular workspace is thus a function of those quantities. Let $\Phi_1 = \Phi_1(l_1, w_1, h_1)$ and $\Phi_2 = \Phi_2(l_2, w_2, h_2)$ be two repective measures for the volumes of W_1 and W_2. A measure on the overall volume of W is given as

$$\Phi = \mu_1\Phi_1 + \mu_2\Phi_2, \quad (4)$$

where μ_i, $i = 1, 2$ are weights assigned to the contributions of W_1 and W_2, respectively.

Let's consider two special cases for (4). (i) When the manipulator possesses no rotational motion, i.e., $W_2 = 0$, or W_2 is fixed as a prescribed rotational regular workspace, the objective function is then reduced to $\Phi = \Phi_1$. The objective of the problem is to maximize the translational regular workspace given that at each point in the translational regular workspace the manipulator at least possesses a rotational capability of W_2. Examples of this type include design of all kinds of translational parallel manipulators (e.g., the 3-UPU manipulator, the DELTA robot, and the Orthoglide) and other k-dof ($k > 3$) manipulators as replacement of translational manipulators. (ii) When no translational motion is allowed, i.e., $W_1 = 0$, or W_1 is fixed as a prescribed translational regular workspace, the size function is reduced to $\Phi = \Phi_2$. Examples of this type include design of rotational parallel manipulators (e.g., the 3-dof spherical manipulator) and its higher-dof replacement. The objective is to maximize rotational workspace at every point in W_1. In this paper, we demonstrate the design technique using the first case only for optimal design of some typical parallel manipulators.

It is a well-known fact that given fixed ranges of actuators of a parallel manipulator, its workspace volume monotonically depends on its overall dimension i.e., the value of α. By considering the constraints due to working environments, we normalize the manipulator dimension so as to find the best design among all normalized manipulators with the same

topology. The result is expected to provide an insight and a basic guidance for practical realization.

$$\sum_{i=1}^{q} \alpha_i = \tau, \tag{5}$$

where τ is a given constant, usually 1, and $\alpha_i \geq 0,\ i = 1, \cdots, q$ are geometric parameters, and usually $q \leq p$. (5) implies that $\alpha_i \in [0, \tau],\ i = 1, \cdots, q$.

B. The workspace constraints

A basic requirement for a regular workspace is that it should be contained in the workspace generated by the resultant manipulator. specifically, it is equivalent to imposing the following constraints to every point $X \in W$,

$$\rho_i^{min} \leq \rho_i(X, \alpha) \leq \rho_i^{max}, \quad i = 1, \cdots, n-m; \tag{6}$$

where ρ_i^{min} and ρ_i^{max} are respectively the lower and upper bound for i-th actuator due to actuator limits and/or mechanical interference between links. Any Cartesian point X is reachable if there exists an inverse kinematic solution θ in the actuator range. The set of such points constituting the Cartesian workspace reachable by the resultant parallel manipulator, which indeed contains the regular workspace W because of (6). In the design algorithm to be introduced later, the regular workspace is discretized and (6) is verified only at nodes in the discretized workspace.

C. The dexterity constraints

In order to guarantee the regular workspace to be effective, constraints on the dexterity index are introduced into the design problem to characterize the quality of the regular workspace. A frequently-used measure for dexterity of a manipulator is the inverse condition number of the kinematic Jacobian matrix, which is defined as

$$\kappa(J) = \frac{\sigma_{min}(J)}{\sigma_{max}(J)},$$

where $\kappa(\cdot)$ denotes the inverse condition number function of matrices, and $\sigma_{min}(\cdot)$ and $\sigma_{max}(\cdot)$ its minimal and maximal singular value functions, respectively. Thus $\kappa \in [0, 1]$.

This performance index has been applied in numerous designs since it characterizes various properties of a manipulator. This measure not only can report an occurrence of *singularity*, but also gives a measure to characterize how far the manipulator is to the nearest singular configuration. The inverse condition number also measures the uniformity of the distribution, or the local *isotropy* characteristic, of the Cartesian velocities and end-effector wrenches. In the force/torque transmission from joints to the end-effector, the inverse condition number also measures the magnitude of the *relative error* of the wrench introduced by the relative error in joint torques and reflect the sensitivity of the wrench due to joint torque error. Given a constant relative error on joint torque, the smaller is the inverse condition number, the larger is the relative error of wrench. If the stiffness in each actuated joint are equal, the stiffness matrix describing the stiffness of the manipulator due to the stiffness at joints is characterized by the product of the kinematic Jacobian and its transpose. The inverse condition number of the Jacobian gives a measure of the uniformity of the Cartesian *stiffness*. Note that if we replace the kinematic Jacobian matrix with the inertial matrix in the dynamic equation, the inverse condition number thus measures the inertial behavior and the isotropy of the acceleration performances [13].

However, when a robot is capable of mixed motions of translational and rotational degrees of freedom or when it is comprised of both rotary and prismatic actuators, elements of the kinematic Jacobian bear different physical units. As a result, a measure such as the inverse condition number of the Jacobian matrix is of little practical significance. Any design based on condition number of kinematic Jacobian will probably produce misleading results. This was first pointed out by Lipkin and Duffy in [14]. Furthermore, even when physical units are uniform, the inverse condition number only evaluates the uniformity of actuator responses given a task-space motion of unit magnitude and arbitrary direction. The non-uniformity of actuator capabilities and/or required task-space response is not taken into account. A usual method to handle this problem is to introduce the concept of *characteristic length* [15] by Tandirci *et al*. and the Jacobian is then normalized by dividing a characteristic length out of all translational elements. Ma and Angeles [16] defined the *natural length* as the characteristic length that produces the best performance measure and applied it in design optimization. When the natural length of a platform manipulator is not derivable, it is approximated by the average platform radius. For a serial manipulator the natural length is calculated by averaging the distances between the operating point and all actuated joint axes by Angeles[17]. In [18], the natural length of a serial manipulator was determined by regarding it as a free design parameter needed to be optimize. This method was later generalized by Stocco, Salcudean, and Sassani [19][20] by pre- and post-multiplying the kinematic Jacobian scaling matrices corresponding to ranges of joint and task-space variables.

Here we introduce a natural and physically meaningful way to scale the Jacobian matrix and make it dimensionally homogeneous by the example of a general Gough-Stewart platform. As shown in Fig. 2, an inertia coordinate frame $O-xyz$ is set up on the base, while a body frame $P-uvw$ is set up on the moving platform with point P being the reference point. A loop-closure equation for the i-th subchain can be derived as

$$\overrightarrow{OP} + \overrightarrow{PB_i} = \overrightarrow{OA_i} + \overrightarrow{A_iB_i}, \quad i = 1, \cdots, 6. \tag{7}$$

Let $\parallel \overrightarrow{OA_i} \parallel = a_i$, $\parallel \overrightarrow{PB_i} \parallel = b_i$, and $\parallel \overrightarrow{A_iB_i} \parallel = \rho_i$, $i = 1, \cdots, 6$. Differentiating (7) with respect to time yields

$$\mathbf{v} + b_i\omega \times \mathbf{r}_i = \rho_i \mathbf{e}_i \times \mathbf{s}_i + \dot{\rho}_i \mathbf{s}_i, \quad i = 1, \cdots, 6, \tag{8}$$

where $\mathbf{v}$ and ω are respectively the translational velocity of the reference point P on the moving platform and the angular velocity of the moving platform both with respect to the inertia frame. $\mathbf{r}_i$ and $\mathbf{s}_i$ are both unit vectors representing the directions along $\overrightarrow{PB_i}$ and $\overrightarrow{A_iB_i}$, respectively, and $\mathbf{e}_i$ denotes

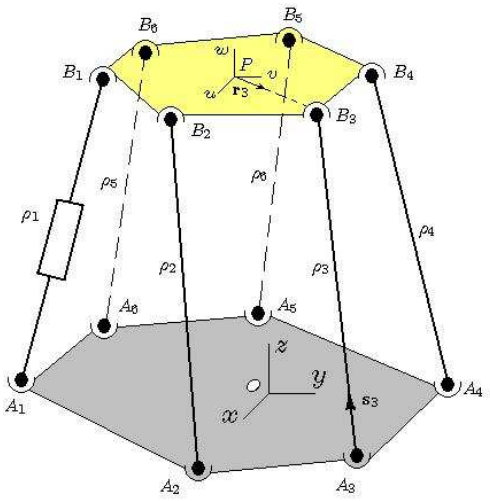

Fig. 2. A schematic of the general Stewart-Gough platform

the angular velocity of the i-th subchain with respect to the inertia frame. To eliminate $\mathbf{e}_i$, we dot-multiply both sides of (8) by $\mathbf{s}_i$ and obtain

$$\mathbf{s}_i^T\mathbf{v} + b_i(\mathbf{r}_i \times \mathbf{s}_i)^T\omega = \dot{\rho}_i, \quad i = 1, \cdots, 6, \tag{9}$$

(9) can then be assembled in matrix form as follows.

$$\dot{\rho} = J\dot{X}, \tag{10}$$

where $\dot{\rho} = [\dot{\rho}_1, \cdots, \dot{\rho}_6]^T$, a vector of the joint velocities, $\dot{X} = [\mathbf{v}^T \ \omega^T]^T$ the vector of Cartesian velocities, and

$$J = \begin{bmatrix} \mathbf{s}_1^T & b_1(\mathbf{r}_1 \times \mathbf{s}_1)^T \\ \mathbf{s}_2^T & b_2(\mathbf{r}_2 \times \mathbf{s}_2)^T \\ \vdots & \vdots \\ \mathbf{s}_6^T & b_6(\mathbf{r}_6 \times \mathbf{s}_6)^T \end{bmatrix}$$

the Jacobian matrix. Clearly the Jacobian J is dimensionally inhomogeneous since the first three columns represent directions of legs and are thus unitless and the remainder three columns carry a unit of length. A natural way of dimensionally homogenizing J is to divide the elements of the i-th row of the last three columns by the corresponding b_i, $i = 1, \cdots, 6$. Thus we have a scaled kinematic Jacobian $\hat{J}$, which is dimensionally homogeneous, as follows.

$$\hat{J} = \begin{bmatrix} \mathbf{s}_1^T & (\mathbf{r}_1 \times \mathbf{s}_1)^T \\ \mathbf{s}_2^T & (\mathbf{r}_2 \times \mathbf{s}_2)^T \\ \vdots & \vdots \\ \mathbf{s}_6^T & (\mathbf{r}_6 \times \mathbf{s}_6)^T \end{bmatrix}.$$

When all passive joints B_i, $i = 1, \cdots, 6$, are arranged on a common sphere centered at P, i.e., $b_i = b$ for all i, a homogeneous Jacobian is obtained through dividing the last three columns of J by a common factor b. This reduces to the case in [21]. For simplicity we may also divide all of the last three columns by the average platform radius $\bar{b} = (\sum_{i=1}^{6} b_i)/6$, which in fact gives an approximation of PB_i, $i = 1, \cdots, 6$, as in [16].

Let $\mathbf{t}_i = \mathbf{r}_i \times \mathbf{s}_i$, $i = 1, \cdots, 6$, we rewrite differential kinematics of the manipulator as follows to see the physical meaning of this method,

$$\dot{\rho} = J_d B\dot{X}, \tag{11}$$

where

$$J_d = \begin{bmatrix} \mathbf{s}_1^T & \mathbf{t}_1^T & & & & \\ & & \mathbf{s}_2^T & \mathbf{t}_2^T & & \\ & & & & \ddots & \\ & & & & \mathbf{s}_6^T & \mathbf{t}_6^T \end{bmatrix}$$

and

$$B = \begin{bmatrix} I & 0 \\ 0 & b_1 I \\ I & 0 \\ 0 & b_2 I \\ \vdots & \vdots \\ I & 0 \\ 0 & b_6 I \end{bmatrix}$$

with I is a 3×3 identity matrix. Clearly J_d is dimensionally homogeneous and B serves as a scaling matrix. We further rewrite the velocity relation as follows,

$$\dot{\rho} = J_d\dot{\hat{X}}, \tag{12}$$

where

$$\dot{\hat{X}} = [\mathbf{v}^T, b_1\omega^T, \mathbf{v}^T, b_2\omega^T, \cdots, \mathbf{v}^T, b_6\omega^T]^T.$$

Note that $b_i\omega$ is the tangential velocity of joint B_i, $i = 1, \cdots, 6$, with respect to the inertia frame, due to the rotational motion of the moving platform. Each pair $(\mathbf{v}, b_i\omega)$ in $\dot{\hat{X}}$ represents a vector of linear velocity at joint B_i, which is composed of the translational velocity $\mathbf{v}$ and the tangential velocity $b_i\omega$ due to angular velocity ω. It is therefore a natural way to deal with the dimensional inhomogeneity problem by dividing the last three columns of the Jacobian J the distances from the joints on the moving platform to the reference point correspondingly.

With the scaled Jacobian $\hat{J}$, the dexterity constraints can be expressed as follows.

$$\kappa(\hat{J}) \geq \gamma, \tag{13}$$

where γ is a constant number specified by users.

Combining (4)-(6) and (13), we formulate the following optimal deisgn problem for maximizing the effective regular workspace.

Problem 1: Optimal Mechanism Design

Find a set of optimal design parameters α such that

$$\max_{\alpha} \quad \Phi(\alpha) \tag{14}$$

$$\text{subject to} \quad \kappa(\hat{J}(X, \theta, \alpha)) \geq \gamma, \tag{15}$$

$$\rho_i^{min} \leq \rho_i(X, \alpha) \leq \rho_i^{max}, \tag{16}$$

$$\varphi_k^{min} \leq \varphi_k(X, \alpha) \leq \varphi_k^{max}, \tag{17}$$

$$\sum_{j=1}^{q} \alpha_j = \tau. \tag{18}$$

where $\forall X \in W$ and $i = 1, \cdots, n-m$. φ_k^{min} and φ_k^{max} are both constants and define a range for the k-th passive joint.

III. Algorithms for the Optimal Design Problem

Clearly the optimal design problem 1 is a constrained nonlinear optimization problem. Two kinds of deterministic algorithms are usually applied to solve this problem. One is the sequential approximation method. Typical representatives of this method are the sequential quadratic programming (SQP) methods. Based on Lagrangian methods, the solution x^* of the nonlinear optimization problem can be obtained by solving , at successive approximations $x^{(i)}$ to x^*, a sequence of corresponding quadratic programming (QP) subproblems. These SQP methods are some of the most efficient algorithms available today. The Dynamic-Q method proposed by Snyman and Hay [22] is also in the category of the sequential approximation method. They are all gradient based methods involving computations of gradient vectors of the objective function and the constraints. Even the computation of Hessian is necessary for applications of SQP methods. The other approach is the transformation methods [23], by which the constrained optimization problem is transformed into an unconstrained one and solved via various unconstrained optimization techniques. A typical representative of this method is the penalty function approach, where extra penalty parameters are introduced.

By observation, neither the objective function (14) nor the dexterity constraint (15) has an explicitly analytical expression with respect to the set of design parameters α. The gradient vectors are thus not readily computed. Furthermore, the objective function in the optimal design problem 1 is generally multimodal, i.e., there may exist several local minima in the feasible region. Those gradient based optimization algorithms are known to converge to local minima. Here, without transformation of the optimization problem, we resort to a direct search method, the random search technique, which was widely studied as a global optimization technique [24]. The algorithms are robust, i.e., they normally work regardless of irregularities of the objective function.

A. The Controlled Random Search Technique

Random search techniques were first proposed by Anderson [25] in 1953 and later by Brooks [26], Rastrigin [27] and Karnopp [12]. Proposals employing random search technique proliferated in the engineering literature. They range from simply simultaneous sampling techniques to more elaborate procedures that involve a coupling of sequential sampling with heuristic hill-climbing methods. The simutaneous sampling procedure is of course very inefficient. Many adaptive or heuristic methods [28][29][30][31][32] [33][34] were thus proposed to improve the efficiency. Solis and Wets [32] and Gelfand and Mitter [35] provided global convergence proofs for two different conceptual algorithms. Random search Techniques have been applied in various fields, such as chemical engineering [36], control[37], circuit design [38], and antenna optimization [39]. Karnopp [12] and other researchers recognized advantages of random search techniques as follows. (1) *Ease of programming and realization*. Anyone can readily apply the technique in his individual application without advanced optimization knowledge. (2) *Robustness*. Practically random search techniques are insensitive to type of objective functions as well as to shape of feasible regions. They're capable of handling of discontinuous, non-differentiable objective functions with a nonconvex feasible region. Some of the techniques are also insensitive to the initial search conditions, such as initial point [40]. (3) *Efficiency*. Although reports [41] showed that random search techniques converge quite slowly in the very close neighborhood of the optimum, they do converge efficiently to within 0.1% of the optimum. And (4) *flexibility*. It is easy to modify the search procedure and combine heuristic knowledge and experience in the algorithm.

In 1978, Goulcher and Long [40] proposed a controlled random search (CRS) method to solve constrained nonlinear optimization problems. Later this method was improved and applied in many chemical plants [36]. The basic philosophy of the method is to select new points by random selection from normal probability distributions centered at the best previous value.

$$\alpha^{(j)} = \alpha^{(j-1)} + \sigma\xi. \tag{19}$$

The equation (19) describes how the new points in j-th iteration, $\alpha^{(j)}$, are generated in the neighborhood of the previous best point $\alpha^{(j-1)}$, where ξ is a vector of random variables ξ_i that is subject to normal probability distribution with zero mean and unity standard deviation as follows.

$$\xi_i \sim N(0,1), \quad i = 1, \cdots, p.$$

$\sigma = \mathrm{diag}(\sigma_1, \cdots, \sigma_p)$ is applied to adaptively modify the standard deviation of the normal probability distribution for every random variable in each iteration. It is actually the standard deviation for the vector of random variables $\sigma\xi$. Therefore, "control" comes by adjustment of the standard deviation of the distribution, which explains the name of the method. Compared with standard optimization techniques, the random variable ξ can be regarded as a search direction, while the standard deviation σ serves as a kind of "step-length", which is adjusted automatically during the search in two situations.

(a) Each time a successful trial has been made. In this case, standard deviations are set according to $\sigma_i = K_1\Delta\alpha_i$, $i = 1, \cdots, p$, where $\Delta\alpha_i$ is a positive quantity describing the distance between the variable's current value α_i and the nearest bound of the variable. $K_1 < 1$ is a compression factor to reduce seach interval and maintain searches in the neighborhood of the best previous point.

(b) After a specified number, typically 100, of consecutive failure. Failure means that no improvement is made with respect to the objective function. When this occurs, for instance, as the optimum is approached, the standard deviations are reduced by

$$(\sigma_i)_{new} = K_2(\sigma_i)_{old}, \quad i = 1, \cdots, p;$$

where $K_2 < 1$ is a positive number.

The basic algorithm of the CRS technique is described as follows.

Algorithm *1:* The basic CRS algorithm

1. Given search intervals, $\alpha_i \in [\underline{\alpha_i}, \overline{\alpha_i}]$, set parameters

K_1, K_2, ϵ, and max_feval denoting the maximum allowable number of function evulation;

2. Generate a feasible initial point $\alpha^{(0)}$ by uniformly random sampling in the given intervals, and compute the corresponding $\Phi^{(0)}$ and $\sigma_i^{(0)} = K_1 \Delta\alpha_i^{(0)}$, $i = 1, \cdots, p$. Set $j = 1$;

3. $k = 1$.

4. If $k > max\_feval$, set $\sigma_{new}^{(j-1)} = K_2 \sigma_{old}^{(j-1)}$ and go to 3; otherwise, generate a new search point by

$$^k\alpha^{(j)} = \alpha^{(j-1)} + \sigma^{(j-1)}\xi.$$

5. If $\Phi(^k\alpha^{(j)}) \leq \Phi^{(j-1)}$, set $k = k+1$, go to 4; otherwise, set $\Phi^{(j)} = \Phi(^k\alpha^{(j)})$ and $\alpha^{(j)} = {}^k\alpha^{(j)}$.

6. Check the stopping criterion

$$\frac{|\alpha_i^{(j)} - \alpha_i^{(j-1)}|}{R_i} \leq \epsilon, \quad i = 1, \cdots, p;$$

where $R_i = \overline{\alpha_i} - \underline{\alpha_i}$. If it is satisfied, end the procedure; otherwise, set $j = j + 1$ and go to 3.

Solis and Wets [32] proved global convergence for their conceptual algorithm, which includes the CRS technique. Their proof needs only minimal technical assumptions, measurability of the objective function f and the feasible set S, that are always satisfied in practice. Readers are referred to the Appendix for detail.

B. The Overall Algorithm

Although the size of maximal effective regular workspace depends uniquely on the design parameters, the real implementation of search of the size involves finding not only the optimal design parameters but also the location of maximal effective regular workspace. There are two schemes to realize the search.

Basicly the first search scheme can be accomplished by two layers of optimization iteration. The outer layer is simply to find the optimal value Φ^* according to the inner layer, the objective function is evaluated at different given design parameters α. Given a set of design parameters α, the inner layer find the maximal size of the effective regular workspace by the following idea. Assume that the shape of the regular workspace is given, say, a cube. Take a point O as its center. Increase the side length of the cube until any of the constraints (15)- (18) is violated. Thus we obtain the maximal size $\Phi^*(O)$ corresponding to center O. Repeating the procedure by choosing different centers and comparing different $\Phi^*(O)$, the maximal size corresponding to the design parameters α, $\Phi^*(\alpha)$, is therefore obtained. Both the outer and inner layers of optimization iterations can be realized by the CRS technique.

In the other scheme the center of the effective regular workspace is directly regarded as part of design parameters. The search of the center of the maximal effective workspace and the search of the optimal design parameters are accomplished simultaneously. There is no difference in result for those two schemes. In the implementation the latter one is employed.

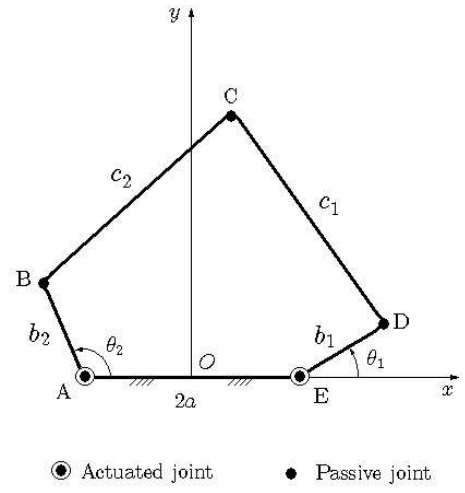

Fig. 3. A schematic for the five-bar parallel linkage

IV. Example 1: Optimal Design of a Five-Bar Parallel Linkage

The five-bar parallel linkage has been applied as a microprobing device [42] and a haptic interface [43]. We consider to design a five-bar parallel linkage as that in [19]. As shown in Fig. 3, all the joints are revolute, and only joints A and E are actuated. A Cartesian coordinate system is set up with the origin O coinciding with the midpoint of AE. Let $\|DE\| = b_1$, $\|AB\| = b_2$, $\|CD\| = c_1$, $\|BC\| = c_2$, and the fixed link $\|AE\| = 2a$. The joint C, with coordinate $X = (x, y)$, is regarded as the reference point of end-effector. The set of design parameters is $\alpha = [a, b_1, b_2, c_1, c_2]^T$.

By geometry of the mechanism, the loop closure equations are derived as follows.

$$(x - a - b_1\cos\theta_1)^2 + (y - b_1\sin\theta_1)^2 = c_1^2; \tag{20}$$

$$(x + a - b_2\cos\theta_2)^2 + (y - b_2\sin\theta_2)^2 = c_2^2. \tag{21}$$

By differentiating the loop closure constraints (20) and (21) with respect to time t, we obtain an instantaneous relationship between the joint rate $\dot\theta$ and the Cartesian velocity $\dot X$.

$$J_x\dot X = J_\theta\dot\theta, \tag{22}$$

where $\dot X = [\dot x, \dot y]^T$, $\dot\theta = [\dot\theta_1, \dot\theta_2]^T$,

$$J_x = \begin{bmatrix} x - a - b\cos\theta_1 & y - b\sin\theta_1 \\ x + a - b\cos\theta_2 & y - b\sin\theta_2 \end{bmatrix}$$

and

$$J_\theta = \begin{bmatrix} by\cos\theta_1 - (x-a)b\sin\theta_1 & 0 \\ 0 & by\cos\theta_2 - (x+a)b\sin\theta_2 \end{bmatrix}.$$

Since the five-bar parallel linkage is a planar positioning device, there is no rotational workspace. Therefore the objective function $\Phi = \Phi_1$. We consider a square shape for the regular workspace and define $\Phi = l$, where l denotes a half of the side length of the effective square workspace. In the simulation, the manipulator size is normalized by $a+b_1+b_2+c_1+c_2 = 1$. The actuation limits are given as $\theta_1 \in [-\frac{\pi}{3}, \frac{2\pi}{3}]$ and $\theta_2 \in [\frac{\pi}{3}, \frac{4\pi}{3}]$. Assume the two rotary actuators are of the same model, which is common in practice, we don't need to scale the Jacobian

a	b_1	b_2	c_1	c_2	x_c	y_c	$\Phi^* = l^*$
0.0070	0.2351	0.2363	0.2593	0.2623	0.0120	0.2368	0.180725

TABLE I

OPTIMAL DESIGN PARAMETERS AND THE OPTIMUM FOR THE FIVE-BAR PARALLEL LINKAGE

a	b	c	y_c	$\Phi^* = l^*$
0.0029	0.4788	0.5182	0.4715	0.371155

TABLE II

OPTIMAL DESIGN PARAMETERS AND THE OPTIMUM FOR THE FIVE-BAR PARALLEL LINKAGE GIVEN IDENTICAL SUBCHAINS

since the Jacobian $J = J_\theta^{-1} J_x$ is dimensionally homogeneous. Suppose a dexterity constraint is given as $\kappa(J) \geq 0.4$. Thus the optimal design problem for maximal effective regular workspace becomes

Problem 2: Optimal design of a five-bar parallel linkage Find a set of optimal design parameters α such that

$$\begin{aligned} \max_{\alpha} \quad & l \\ \text{subject to} \quad & \kappa(J(X,\theta,\alpha)) \geq 0.4, \\ & -\frac{\pi}{3} \leq \theta_1(X,\alpha) \leq \frac{2\pi}{3}, \\ & \frac{\pi}{3} \leq \theta_2(X,\alpha) \leq \frac{4\pi}{3}, \\ & a + b_1 + c_1 + b_2 + c_2 = 1. \\ & a,\ b_1,\ b_2,\ c_1,\ c_2 \in [0,1] \end{aligned}$$

where $\forall X \in W$.

Here the center of the square-shaped workspace (x_c, y_c) is regarded as independent variables. considering the size constraint, there're totally 6 independent variables.

Table I gives the optimum of the objective function and its corresponding optimal design parameters and the center. It is easy to find that the resultant optimal design parameters suggest two geometrically identical subchains since $b_1 \approx b_2$ and $c_1 \approx c_2$. Therefore we consider another design with an assumption of identical subchains. Let $b_i = b$ and $c_i = c$, $i = 1, 2$. The center of square workspaces is specified as $(0, y_c)$ because of the symmetric architecture. And the manipulator is normalized by $a + b + c = 1$. By redoing the optimization we obtain optimal design parameters and the corresponding optimal objective as shown in Table II.

In order to measure space utilization of a manipulator, we define a *space utilization index* (SUI) as the ratio of the side length of the maximum effective workspace to the total length of a subchain, which generally characterizes the size of a manipulator. In the case of the design of the nonsymmetric five-bar parallel linkage, the space utilization index is given as

$$SUI = \frac{2l^*}{a + b_1 + c_1} \quad \text{or} \quad \frac{2l^*}{a + b_2 + c_2}. \tag{23}$$

Thus $SUI = 71.5\%$. For the symmetric design case, $SUI = 2l^*/(a+b+c) = 74.2\%$, which is larger than that of the nonsymmetric design case. This shows a symmetric architecture is desirable for our design requirements.

Fig. 4 shows the workspace generated by the optimal symmetric design, where the region enclosed by the square is the maximum effective square workspace. A distribution of inverse condition number of J in the maximal effective square workspace is shown in Fig. 5-(a). And Fig. 5-(b) shows its contour plot. From the figure of workspace containment, we

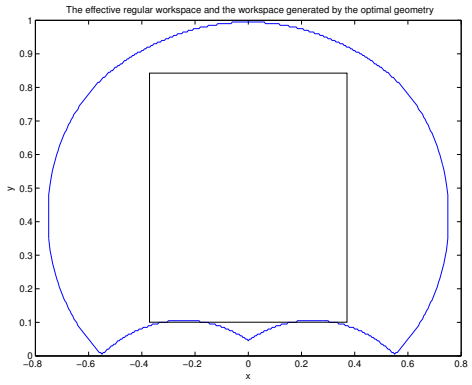

Fig. 4. The workspace generated by the optimal geometry

find a little portion of the effective regular workspace lies out of the workspace generated by the resulting optimal linkage with constraints of actuation limits. Also the minimal inverse condition number in the effective regular workspace is 0.3966, which is a little smaller than the prescribed value $\gamma = 0.4$. Both constraints (15) and (16) are violated. This is simply because we use only typical discrete points in the Cartesian regular workspace to represent constraints on all points over the regular workspace (15) and (16). This of course introduces some errors. However, the errors are rather small and they're even acceptable in real engineering design. Furthermore, we can eliminate the effects of discretization of regular workspace by applying a little bit stricter constraints of (15) and (16), say a little bit larger γ and a little bit smaller ranges for actuation.

From the optimal design parameters in Table I, the manipulator demonstrates two nearly identical subchains in geometry, which verifies that our usual *symmetric* five-bar linkage is a good design. Also the design parameter a tends to zero, which implies the coincidence of the actuation points A and E. This is consistent with our common sense that when a parallel manipulator degenerates to a serial one, it gives a largest workspace. In practice a minimal value of a should be

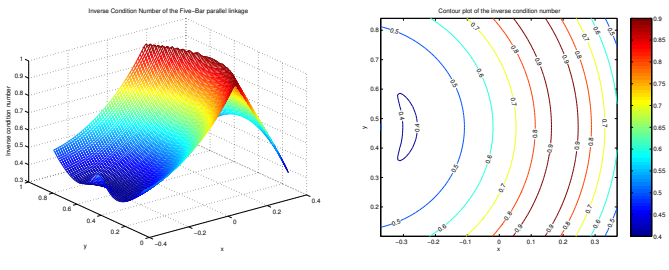

(a) (b)

Fig. 5. (a) Inverse condition number in the maximal effective regular workspace; (b) A contour plot for the inverse condition number in the maximal effective regular workspace.

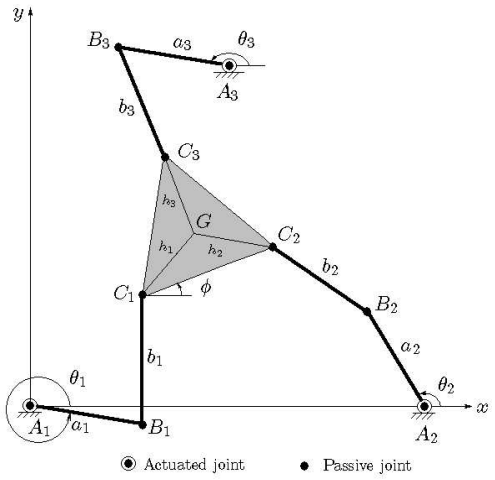

Fig. 6. A schematic of the 3-RRR planar parallel manipulator

provided as a lower bound for search such that the resultant optimal manipulator is practically realizable.

V. Example 2: optimal design of a 3-RRR planar parallel manipulator

The five-bar parallel linkage is a planar translational manipulator that doesn't possess orientational motion. Here we consider a planar parallel manipulator involving motions of both translation and rotation, a 3-RRR planar parallel manipulator, which was widely-studied in many literatures [8]. Note the underlined "R" denotes an *actuated* revolute joint.

A schematic of the 3-RRR planar parallel manipulator is shown in Fig. 6. All joints are of the revolute type, and the three actuators A_1, A_2, A_3 are fixed. The manipulator consists of 3 subchains, namely $A_iB_iC_i$, $i = 1, 2, 3$, which connect to the moving platform $C_1C_2C_3$ in parallel. Only joints A_i, $i = 1, 2, 3$ are actuated, while B_i and C_i, $i = 1, 2, 3$ are all passive joints. As shown in Fig. 6, a Cartesian coordinate system is set up with the origin being coincident with point A_1. A loop closure equation can thus be derived for each subchain as follows.

$$\overrightarrow{A_iG} + \overrightarrow{GC_i} = \overrightarrow{A_iB_i} + \overrightarrow{B_iC_i}, \quad i = 1, \cdots, 3, \tag{24}$$

where G is the reference point on the moving platform $C_1C_2C_3$. Let $a_i = \|A_iB_i\|$, $h_i = \|GC_i\|$, $i = 1, \cdots, 3$, a velocity vector-loop equation is obtained by taking the derivative of (24) with respect to time and some simple manipulations:

$$\mathbf{b}_i^T\mathbf{v} + \dot{\phi}\mathbf{k}^T(\mathbf{h}_i \times \mathbf{b}_i)h_i = \dot{\theta}_i\mathbf{k}^T(\mathbf{a}_i \times \mathbf{b}_i)a_i, \tag{25}$$

for $i = 1, \cdots, 3$, where $\mathbf{v}$ is the translational velocity of the reference point G on the moving platform, $\dot{\phi}$ is the angular velocity of the moving platform, both with respect to the fixed frame, and $\mathbf{a}_i$, $\mathbf{b}_i$, $\mathbf{h}_i$, and $\mathbf{k}$ are all unit vectors along $\overrightarrow{A_iB_i}$, $\overrightarrow{B_iC_i}$, $\overrightarrow{GC_i}$, and z-axis, respectively. Stacking the three scalar equations in (25), we have differential kinematics in matrix form as follows.

$$J_x\dot{X} = J_\theta\dot{\theta}, \tag{26}$$

where J_x and J_θ are forward Jacobian and inverse Jacobian, respectively, and $X = [x\ y\ \phi]^T$, $\theta = [\theta_1\ \theta_2\ \theta_3]^T$, $\dot{X} = [\mathbf{v}^T\ \dot{\phi}]^T$, and $\dot{\theta} = [\dot{\theta}_1\ \dot{\theta}_2\ \dot{\theta}_3]^T$, and

$$J_x = \begin{bmatrix} \mathbf{b}_1^T & \mathbf{k}^T(\mathbf{h}_1 \times \mathbf{b}_1)h_1 \\ \mathbf{b}_2^T & \mathbf{k}^T(\mathbf{h}_2 \times \mathbf{b}_2)h_2 \\ \mathbf{b}_3^T & \mathbf{k}^T(\mathbf{h}_3 \times \mathbf{b}_3)h_3 \end{bmatrix}$$

and

$$J_\theta = \begin{bmatrix} \mathbf{k}^T(\mathbf{a}_1 \times \mathbf{b}_1)a_1 & 0 & 0 \\ 0 & \mathbf{k}^T(\mathbf{a}_2 \times \mathbf{b}_2)a_2 & 0 \\ 0 & 0 & \mathbf{k}^T(\mathbf{a}_3 \times \mathbf{b}_3)a_3 \end{bmatrix}.$$

The kinematic Jacobian can thus be obtained by $J = J_\theta^{-1}J_x$. Clearly the Jacobian J is dimensionally inhomogeneous since elements in J_θ bear uniform physical units, while in J_x the elements of the first two columns are unitless and those in the third columns have a unit of length. By discussions in Section II-C, we homogenize the Jacobian J by dividing the elements in its third column with corresponding h_i and therefore obtain a dimensionally homogeneous Jacobian $\hat{J}$.

For ease of manufacturing and general-purpose applications, a symmetric structure is applied for the 3-RRR parallel manipulator as in [8], i.e. (i) all three subchains are identical in geometry; (ii) the three actuated joints are arranged in such a way that they, as vertices, constitute an equilateral triangle $\Delta A_1A_2A_3$; and (iii) the triangle consisting of the three passive joints on the moving platform as its vertices is equilateral. Let $a_i = a$ and $b_i = b$ for $i = 1, \cdots, 3$, and $\|A_iA_j\| = c$, $i, j = 1, \cdots, 3$, $i \neq j$. Thus the vector of design parameters becomes $\alpha = [a\ b\ h\ c]^T$. The manipulator size is normalized by $a + b + h = 1$. Let's consider a regular workspace W with a prescribed rotational workspace $[-\phi_0, \phi_0]$ and a prescribed square shape for the translational workspace W_1. This requires that at each point of W_1 the manipulator at least has a orientational capability of $[-\phi_0, \phi_0]$. In the simulation $\phi_0 = 30^\circ$. Given the center of $\Delta C_1C_2C_3$ being taken as the reference point G, the maximal effective regular workspace will centered at $[\frac{c}{2}, \frac{\sqrt{3}c}{6}, 0]$, which coincides with the center of $\Delta A_1A_2A_3$ at $\phi = 0$. This is because the translational workspace of the symmetric manipulator is symmetric about the center of $\Delta A_1A_2A_3$ at $\phi = 0$. By taking $\Phi = l$, where l denotes a half of the side length of the effective square translational workspace, we formulate the optimal design problem for maximization of the effective regular workspace as follows.

Problem 3: Optimal design of a 3-RRR planar parallel manipulator

Find a set of optimal design parameters α such that

$$\begin{aligned} \max_{\alpha} \quad & l \\ \text{subject to} \quad & \kappa(\hat{J}(X, \theta, \alpha)) \geq 0.2; \\ & -\frac{\pi}{3} \leq \theta_1(X, \alpha) \leq \frac{\pi}{3}; \\ & \frac{\pi}{3} \leq \theta_2(X, \alpha) \leq \pi; \\ & \pi \leq \theta_3(X, \alpha) \leq \frac{5\pi}{3}; \\ & a + b + h = 1; \\ & a,\ b,\ h \in [0, 1], \quad c \in [0, 2]; \end{aligned}$$

a	b	h	c	$\Phi^* = l^*$
0.5279	0.4718	0.0003	1.0157	0.205750

TABLE III

OPTIMAL DESIGN PARAMETERS AND THE OPTIMUM FOR THE 3-RRR PLANAR PARALLEL MANIPULATOR

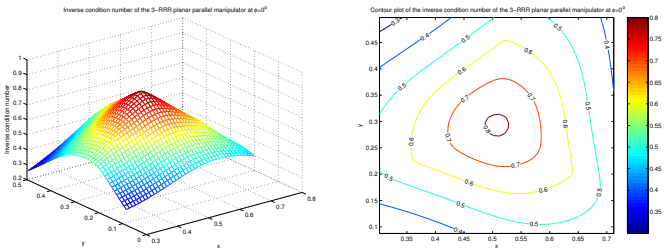

(a) (b)

Fig. 7. (a) Inverse condition number of $\hat{J}$ at $\phi = 0^{\rm o}$; (b) Contour plot of the inverse condition number of $\hat{J}$ at $\phi = 0^{\rm o}$.

where $\forall X \in W$. Note that actuation limits are provided for practical reasons.

The optimal design parameters and its corresponding maximal size of the effective square translational workspace is given in Table III. Note the resulting manipulator has a moving platform with very small size ($h = 0.0003$), which indicates a zero-size of the moving platform is desirable for the maximization of effective regular workspace. This coincides with design results in [8].

Fig. 7-9 show distributions and contour plots of inverse condition number in the maximal effective square workspace when $\phi = 0^{\rm o}$, $-30^{\rm o}$, and $30^{\rm o}$, respectively. The minimal value of κ over the maximal effective workspace is 0.1999, which is a little smaller than the prescribed one, 0.2. Fig. 10 shows the translational workspace cross section generated by the resulting optimal design at $\phi = 0^{\rm o}$. The shaded square region represents the cross section of the maximal effective translational workspace at $\phi = 0^{\rm o}$. It is completely contained in the manipulator's workspace and is far from the boundary, which indicates that only the dexterity constraint (15) takes effect. since the size of the moving platform is very small, it affects little on translational workspace. Therefore, workspace cross sections generated at different orientations are almost the same.

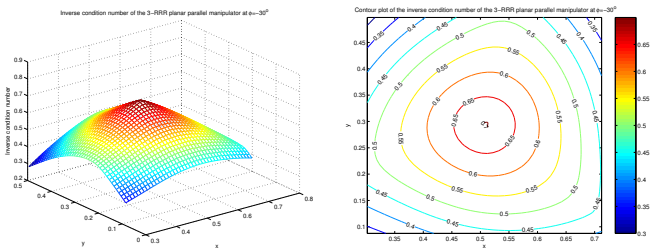

(a) (b)

Fig. 8. (a) Inverse condition number of $\hat{J}$ at $\phi = -30^{\rm o}$; (b) Contour plot of the inverse condition number of $\hat{J}$ at $\phi = -30^{\rm o}$.

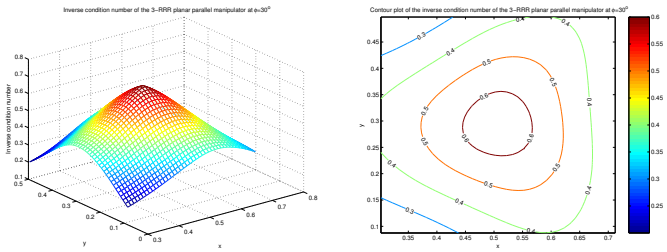

(a) (b)

Fig. 9. (a) Inverse condition number of $\hat{J}$ at $\phi = 30^{\rm o}$; (b) Contour plot of the inverse condition number of $\hat{J}$ at $\phi = 30^{\rm o}$.

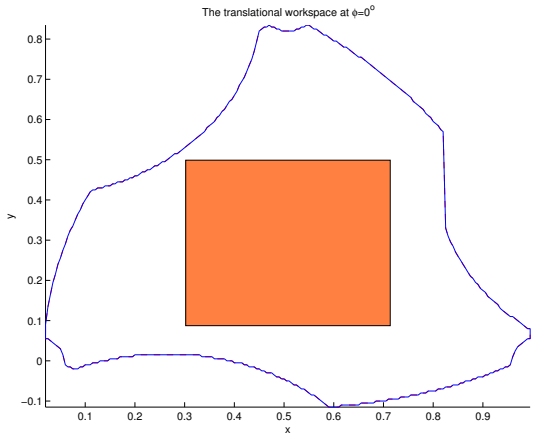

Fig. 10. The workspace generated by the optimal geometry

VI. EXAMPLE 3: OPTIMAL DESIGN OF A ROTATIONAL DELTA ROBOT

In this section we consider a spatial parallel manipulator with purely translational motion, the rotational DELTA robot, as shown in Fig. 11. This architecture was invented by Clavel [44] and is well-known due to its very high speed. The mechanism consists of a base, a moving platform, and three identical subchains connecting them together in parallel. All the three subchains have the same $\underline{\rm R}{\rm R}P_a{\rm R}$ topology from base to the moving platform, where R denotes a *revolute* joint, P_a a *parallelogram*, and the underscored "R" an actuated revolute joint. The three actuated joints on the base are arranged symmetrically, i.e. they, each being a vertex, constitute an equilateral triangle. So do the three passive joints on the moving platform. The kinematic parameters are depicted in Fig. 12 for a rotational DELTA robot, where a_i denotes the length of upper leg A_iB_i, b_i the length of the parallelogram, and $R_i = \|OA_i\|$, $r_i = \|PC_i\|$, $i = 1, \cdots, 3$, with O a point on the base and P a reference point on the moving platform.

Let $a_i = a$, $b_i = b$, $R_i = R$, $r_i = r$, $i = 1, \cdots, 3$ for our symmetrical arrangement with identical subchains and O and P be centers of the base and moving platform equilateral triangles, respectively. An inertia frame is set up with the origin coinciding with the base center O, the base triangle being in the xy-plane, and OA being in the $+x$-axis. The $+z$-axis points up and is perpendicular to the base triangle. The reference point $P = (x, y, z)$ represents the motion of the moving platform. It is easy to derive three loop constraints as

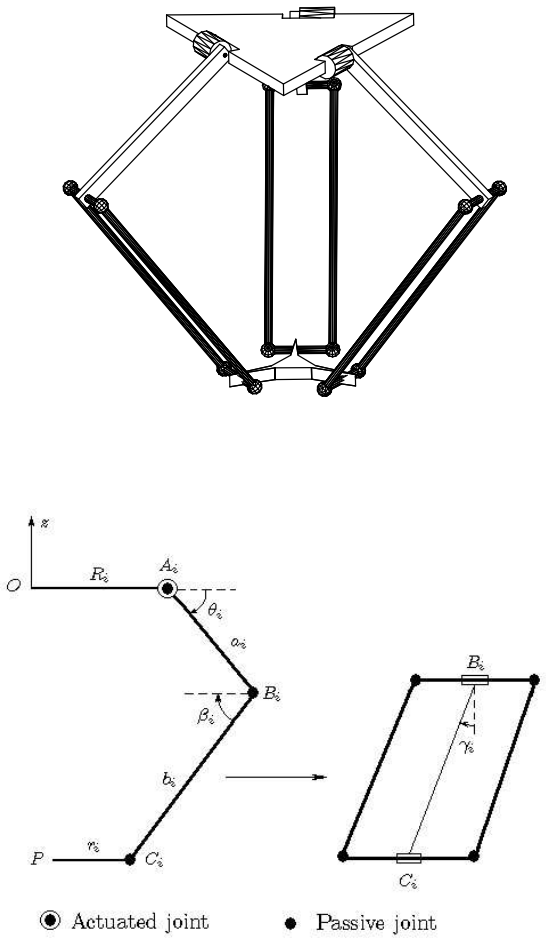

Fig. 12. A subchain of the rotational DELTA robot

follows.

$$(x + (d - a\cos\theta_i)\cos\varphi_i)^2 + (y + (d - a\cos\theta_i)\sin\varphi_i)^2 + (z + a\sin\theta_i)^2 - b^2 = 0 \quad (27)$$

for $i = 1, \cdots, 3$, where θ_i is the i-th actuator angle, and $d = R - r$. In the expressions φ_i denotes the relative angle displacement between the i-th subchain and the $+x$-axis. In our symmetric arrangement, $\varphi_i = (i-1)\frac{2\pi}{3}$ for $i = 1, \cdots, 3$.

Differentiating the loop constraints (27) with respect to time t we obtain the relationship $J_x\dot{X} = J_\theta\dot{\theta}$ between joint rate and Cartesian velocities with

$$J_x = \begin{bmatrix} v_1^T \\ v_2^T \\ v_3^T \end{bmatrix}, \quad (28)$$

where $v_i = [x + (d - a\cos\theta_i)\cos\varphi_i, \ y + (d - a\cos\theta_i)\sin\varphi_i, \ z + a\sin\theta_i]^T$, $i = 1, \cdots, 3$, and

$$J_\theta = -\mathrm{diag}(d_1, d_2, d_3), \quad (29)$$

where $d_i = (x\cos\varphi_i + y\sin\varphi_i + d)a\sin\theta_i + za\cos\theta_i$ for $i = 1, \cdots, 3$. Thus we have a dimensionally homogeneous kinematic Jacobian $J = J_\theta^{-1}J_x$. If all actuators are identical and force/velocity requirements on x, y, z-axis are the same, we don't need to scale the Jacobian and use it directly in the optimization.

In the design we consider a cubic shape for the regular workspace W and let $\Phi = l$, where l is the side length of the cubic workspace. The center of the resultant maximal effective regular workspace is indetermined and is regarded as design parameters. However, the center should be in the z-axis, i.e. $(0, 0, z_c)$, since the manipulator is symmetric with respect to the z-axis. Therefore a set of design parameters is determined, $\alpha = [a\ b\ d\ z_c]^T$, and the manipulator size is normalized using $a + b + d = 1$. Certain limits are imposed on the actuated and passive joints as in [45]. (a) $-40^\mathrm{o} \le \gamma_i \le 40^\mathrm{o}$ due to constructional constraints on the parallelogram's articulations; (b) $45^\mathrm{o} \le \theta_i + \beta_i \le 180^\mathrm{o}$ is imposed in order to avoid interference between the upper legs and the parallelogram rods when the angle is acute and to avoid ambiguities in computation; and (c) $-30^\mathrm{o} \le \theta_i \le 100^\mathrm{o}$ is chosen. Given a requirement on the dexterity of the resulting manipulator and combining all other requirements, the optimal design problem is formulated as follows.

Problem 4: Optimal design of a rotational DELTA robot Find a set of optimal design parameters α such that

$$\begin{aligned} \max_{\alpha} \quad & l \\ \text{subject to} \quad & \kappa(J(X,\theta,\alpha)) \ge 0.4; \\ & -30^\mathrm{o} \le \theta_i(X,\alpha) \le 100^\mathrm{o}; \\ & 45^\mathrm{o} \le \theta_i + \beta_i \le 180^\mathrm{o}; \\ & -40^\mathrm{o} \le \gamma_i \le 40^\mathrm{o}, \ i = 1, \cdots, 3; \\ & a + b + d = 1; \\ & a, \ b, \ d \in [0,1], \quad z \in [-1, 0]; \end{aligned}$$

where $\forall X \in W$.

The optimal values of design parameters and the corresponding maximal size of effective regular workspace are given in Table IV. We can see that d tends to zero, which indicates that a same size of the base and the moving platform is desirable for maximization of the effective regular workspace. This tallies with our intuition.

Fig. 13-15 show distribution of inverse condition number at cross sections of $z = z_c$, $z = z_c - l^*$, and $z = z_c + l^*$ of the maximal effective cubic workspace. The minimal κ in the maximal effective regular workspace is 0.3997, which is a little less than the prescribed one, 0.4. Considering the joint limits, the workspace generated by the DELTA robot is the intersection of a right hexigonal prism with infinite hight and three identical revolution volumes with different axes, as shown in [44]. Fig. 16 shows workspace cross sections generated by the resulting DELTA robot respectively at $z = z_c - l^*$ and $z = z_c$, while Fig. 17 shows the workspace cross section at $z = z_c + l^*$. The regions enclosed by squares in the figures correspond to cross sections of the maximal effective regular workspace. Clearly, in the Fig. 16 only the limits on γ_i take effects, while in the Fig. 17 the workspace constraints become effective. In the Fig. 16 the maximal effective regular workspace cross sections are perfectly contained in the resulting workspace, while in the Fig. 17 the cross section of the maximal effective regular workspace goes beyond the boundary of the resulting workspace a little. This and the

a	b	d	z_c	$\Phi^* = l^*$
0.5837	0.4064	0.0099	-0.6889	0.129578

TABLE IV

OPTIMAL DESIGN PARAMETERS AND THE OPTIMUM FOR THE DELTA ROBOT

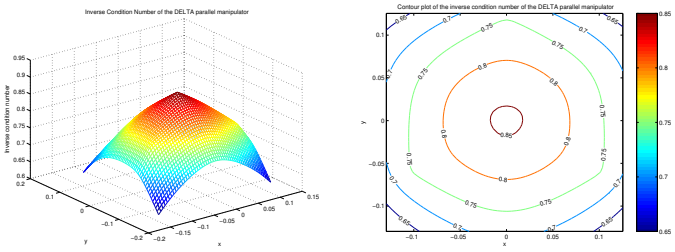

(a) (b)

Fig. 13. (a) Inverse condition number of J at $z = z_c$; (b) Contour plot of the inverse condition number of J at $z = z_c$.

small minimal κ are simply because only some representative discrete points (in this example, only 9 points, the 8 vertices and the center) are chosen to express the constraints. However, an adjustment of the bounds of the constraints or a selection of more representative points will lead to better results.

VII. EXAMPLE 4: OPTIMAL DESIGN OF A GENERAL STEWART-GOUGH PLATFORM

In this section we consider to optimally design a commonly-used Stewart-Gough platform, as shown in Fig. 18, which is capable of 6-dof motion consisting of a 3-dof translational and a 3-dof orientational motion. The manipulator is composed of two platforms, the base (the lower one) and the moving platform (the upper one), and six identical extensible legs in parallel connecting them together. Each leg consists of three joints, which in serial are $S\underline{P}S$ from base to the moving platform, where S denotes a **s**pherical joint while P is a **p**rismatic joint. Both the spherical joints are passive. Only the P-joint is actuated to extend/retract the leg. Note the first S-joint can be substituted by a universal joint without changing motion of the moving platform.

Assume that the six joints on the base are coplanar and constitute a semiregular hexagon, so do the six joints on the moving platform. Their relative arrangement is shown in Fig. 18. An inertia frame $O - xyz$ is set up at the center

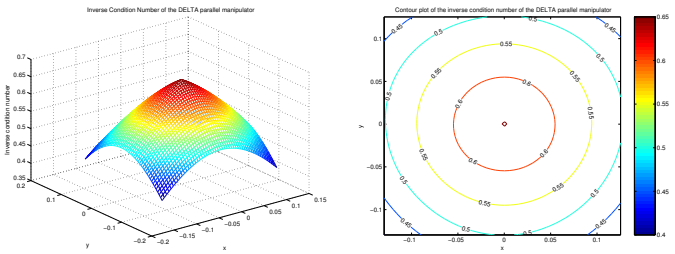

(a) (b)

Fig. 14. (a) Inverse condition number of J at $z = z_c - l^*$; (b) Contour plot of the inverse condition number of J at $z = z_c - l^*$.

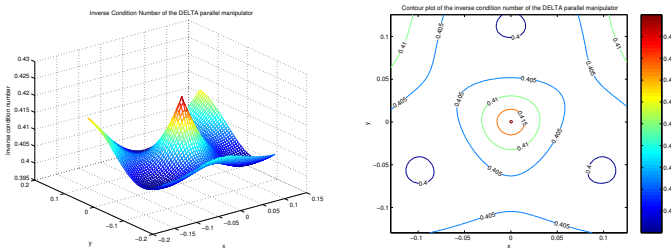

(a) (b)

Fig. 15. (a) Inverse condition number of J at $z = z_c + l^*$; (b) Contour plot of the inverse condition number of J at $z = z_c + l^*$.

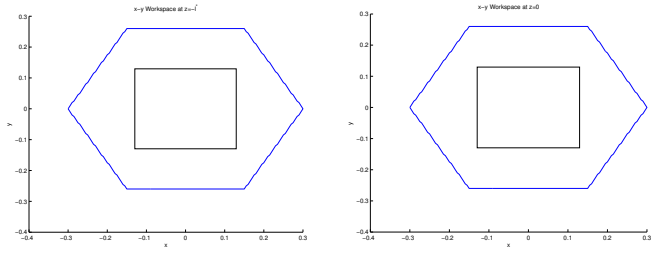

(a) (b)

Fig. 16. (a) xy workspace cross section at $z = z_c - l^*$; (b) xy workspace cross section at $z = z_c$.

of the base with the z-axis pointing vertically upward. A body frame $P - uvw$ is attached to the center of the moving platform with the w-axis normal to the platform, pointing outward. The frames are set up such that the x-axis passes both midpoints of A_1A_2 and A_4A_5 perpendicularly, and u-axis passes both midpoints of B_1B_2 and B_4B_5 perpendicularly. At the home position the body frame is assumed to have the same orientation as the inertia frame.

We denote the lengths of the extensible legs by $\rho_1, \cdots, \rho_6$ with $\rho_i = \|A_iB_i\|$, $i = 1, \cdots, 6$. Let $\|OA_i\| = a$, $\|PB_i\| = b$, $i = 1, \cdots, 6$. Let C_i be the mid-point of A_iA_{i+1}, and D_i be the mid-point of B_iB_{i+1}, $i = 1, \cdots, 6$. Therefore $\angle C_iOC_{i+1} = \frac{\pi}{3}$, $\angle C_iOC_{i+2} = \frac{2\pi}{3}$, and $\angle D_iOD_{i+1} = \frac{\pi}{3}$, $\angle D_iOD_{i+2} = \frac{2\pi}{3}$, $i = 1, \cdots, 6$. Here we identify A_j with A_i given $j = i + 6n$ and i, j, n all natural numbers.

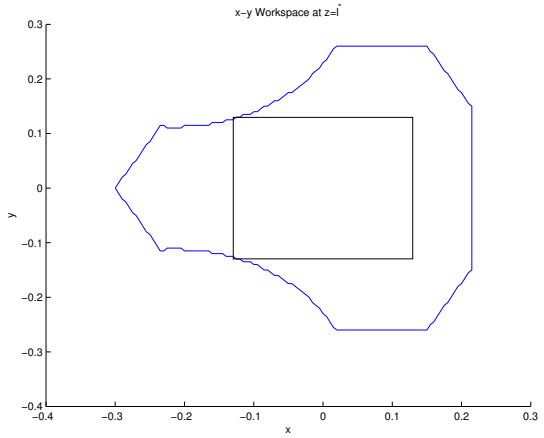

Fig. 17. xy workspace cross section at $z = z_c + l^*$

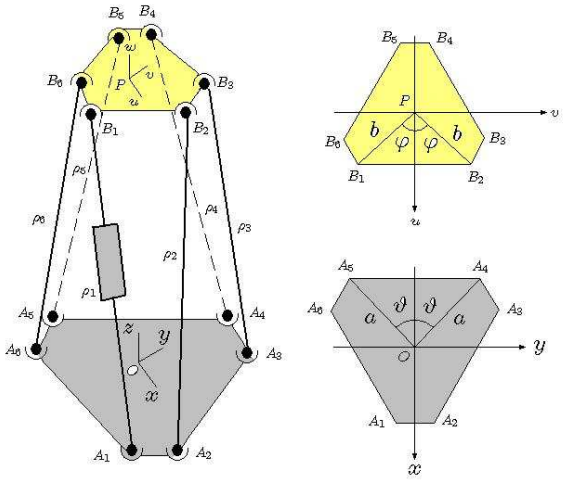

Fig. 18. A schematic for the commonly used Stewart-Gough platform

Let $\varphi = \frac{1}{2}\angle B_iPB_{i+1}$, $i = 1, 3, 5$, and $\vartheta = \frac{1}{2}\angle A_iOA_{i+1}$, $i = 2, 4, 6$. Assume $A_0 = [a\ 0\ 0]^T$ and $B_0 = [b\ 0\ 0]^T$, we find the coordinate for A_i with respect to frame $O - xyz$,

$$A_i = R_z(\xi_i(\vartheta))A_0, \quad i = 1, \cdots, 6 \tag{30}$$

where $R_z(\cdot)$ is a transformation matrix representing a rotation about the z-axis a certain angle, and $\xi_i(\vartheta)$ denotes the angle made by the $+x$-axis and the vector OA_i counterclockwise and is a function of ϑ. Similarly, with respect to the body frame $P - uvw$, the coordinates of B_i are given as follows.

$$B_i^b = R_w(\zeta_i(\varphi))B_0, \quad i = 1, \cdots, 6 \tag{31}$$

where $R_w(\cdot)$ denotes a rotation about the w-axis a certain angle, and $\zeta_i(\varphi)$ represents the angle made by the $+u$-axis and the vector PB_i counterclockwise. Note the superscript b denotes a coordinate with respect to the body frame.

The configuration of the moving platform can be described by both the position of the reference point $P = (x, y, z)$ and the orientation of the moving platform (ϕ,β,ψ), which are the ZYX Euler angles. The orientation of the body frame $P-uvw$ is obtained by the following sequence of rotations from the inertial frame $O - xyz$, first rotate frame $P - uvw$ about the u-axis in the body frame an angle ϕ (roll), then about the v-axis in the (resulting) body frame an angle β (pitch), and finally about w-axis in the (resulting) body frame an angle ψ (yaw). The orientation matrixs can be represented by

$$R = \begin{bmatrix} c_\beta c_\psi & -c_\phi s_\psi + s_\phi s_\beta c_\psi & s_\phi s_\psi + c_\phi s_\beta c_\psi \\ c_\beta s_\psi & c_\phi c_\psi + s_\phi s_\beta s_\psi & -s_\phi c_\psi + c_\phi s_\beta s_\psi \\ -s_\beta & s_\phi c_\beta & c_\phi c_\beta \end{bmatrix}.$$

Here s_ϕ, c_ϕ are abbrevations for $\sin\phi$ and $\cos\phi$, respectively, and similar for the other terms. Therefore the homogeneous transformation from positions in body frame to the inertia frame is described by the transformation matrix as follows.

$$g = \begin{bmatrix} R & p \\ 0 & 1 \end{bmatrix}$$

where $p = [x\ y\ z]^T$, the position of the P with respect to the inertia frame $O - xyz$. The homogeneous expression of the coordinate of B_i with respect to the inertia frame can expressed as follows.

$$B_i^h = gB_i^{bh} \tag{32}$$

where the superscript h denotes an homogeneous expression and B_i^{bh} represents the homogeneous expression of B_i^b, which is obtained by appending an element 1 to the end of B_i^b. Therefore a loop-closure equation can be derived from $\|A_iB_i\| = \rho_i$ or

$$\rho_i^2 = A_iB_i^TA_iB_i = (gB_i^{bh} - A_i)^T(gB_i^{bh} - A_i).$$

Let $F_i = (gB_i^{bh} - A_i)$. Differentiating the equation above for $i = 1, \cdots, 6$ and stacking them together, we obtain differential kinematics of the Stewart-Gough platform.

$$J_\rho\dot{\rho} = J_x\dot{X} \tag{33}$$

where $\dot{\rho} = [\dot{\rho}_1, \cdots, \dot{\rho}_6]^T$, $\dot{X} = [\dot{x}\ \dot{y}\ \dot{z}\ \dot{\phi}\ \dot{\beta}\ \dot{\psi}]^T$, $J_\rho = \mathrm{diag}\{\rho_1, \cdots, \rho_6\}$ and

$$J_x = \begin{bmatrix} F_1^T\frac{\partial g}{\partial x}\mathbf{b}_1 & F_1^T\frac{\partial g}{\partial y}\mathbf{b}_1 & F_1^T\frac{\partial g}{\partial z}\mathbf{b}_1 & F_1^T\frac{\partial g}{\partial \phi}\mathbf{b}_1 & F_1^T\frac{\partial g}{\partial \beta}\mathbf{b}_1 & F_1^T\frac{\partial g}{\partial \psi}\mathbf{b}_1 \\ F_2^T\frac{\partial g}{\partial x}\mathbf{b}_2 & F_2^T\frac{\partial g}{\partial y}\mathbf{b}_2 & F_2^T\frac{\partial g}{\partial z}\mathbf{b}_2 & F_2^T\frac{\partial g}{\partial \phi}\mathbf{b}_2 & F_2^T\frac{\partial g}{\partial \beta}\mathbf{b}_2 & F_2^T\frac{\partial g}{\partial \psi}\mathbf{b}_2 \\ \vdots & \vdots & \vdots & \vdots & \vdots & \vdots \\ F_6^T\frac{\partial g}{\partial x}\mathbf{b}_6 & F_6^T\frac{\partial g}{\partial y}\mathbf{b}_6 & F_6^T\frac{\partial g}{\partial z}\mathbf{b}_6 & F_6^T\frac{\partial g}{\partial \phi}\mathbf{b}_6 & F_6^T\frac{\partial g}{\partial \beta}\mathbf{b}_6 & F_6^T\frac{\partial g}{\partial \psi}\mathbf{b}_6 \end{bmatrix}$$

where $\mathbf{b}_i = B_i^{bh}$. Therefore the kinematic Jacobian can be derived by $J = J_\theta^{-1}J_x$. Since the Jacobian J is dimensionally inhomogeneous, the elements in the last three columns of J are divided by b and a dimensionally homogeneous Jacobian $\hat{J}$ is obtained, as discussed in Section II-C.

Similar to the example of the 3-RRR parallel manipulator, the effective regular workspace of the Stewart-Gough platform is composed of two portions, the translational one W_1 and the rotational one W_2. Here we maximize the translational portion while fix the rotational portion as a prescribed rotational workspace. In other words, for every point in the translational portion, the manipulator is required to have a rotational workspace at least containing the rotational portion. Here we require the manipulator at least have a rotational capability of $W_2 = [\phi_0, \phi_1] \times [\beta_0, \beta_1] \times [\psi_0, \psi_1]$ in W_1, where ϕ_0 and ϕ_1 are respectively the lower and upper bounds for the Euler angle ϕ, and similar case for the other terms. This is a usual requirement in practical design.

Let's still consider a cubic shape for the translational regular workspace W_1 and let l be its side length, the objective function is thus $\Phi = l$. The actuation limits are normalized and given as $\Delta\rho_i \in [0, 1]$, $i = 1, \cdots, 6$. A constraint on the manipulator size is given as $a + \rho_0 + b = \lambda$, where ρ_0 is the leg length at home position (where all leg are half actuated), and λ a given constant representing the relative size of the manipulator with respect to the actuation length. In the simulation, $\lambda = 2$. The center of the maximal cubic workspace is given as $(0, 0, z_c, 0, 0, 0)^T$ since the manipulator is architecturally symmetric about the z-axis. Thus the set of design parameters is $\alpha = [a\ b\ \rho_0\ \vartheta\ \varphi\ z_c]$. The dexterity requirement is given as $\kappa \geq \gamma$ with $\gamma = 0.2$. The optimal design of a Stewart-Gough platform is given as follows.

a	b	ρ_0	ϑ	φ	z_c	$\Phi^* = l^*$
0.6153	0.0631	1.3216	1.0419	1.0416	1.1955	0.2914

TABLE V
OPTIMAL DESIGN PARAMETERS AND THE OPTIMUM FOR THE STEWART-GOUGH PLATFORM

Problem 5: Optimal design of a Stewart-Gough platform

Find a set of optimal design parameters α such that

$$\begin{aligned} \max_{\alpha} \quad & l \\ \text{subject to} \quad & \kappa(\hat{J}(X,\theta,\alpha)) \geq 0.2; \\ & \rho_0 - 0.5 \leq \rho_i(X,\alpha) \leq \rho_0 + 0.5; \\ & a + b + \rho_0 = 2; \\ & a,\ b, z_c \in [0,2], \quad \rho_0 \in [0.5,2], \quad \vartheta,\ \varphi \in [0, \frac{\pi}{3}]; \end{aligned}$$

for all $X \in W$ and $i = 1, \cdots, 6$.

Using the CRS algorithm, we obtain the optimal values of the design parameters and their corresponding optimum as shown in Table V. If we define the *actuation efficiency* as ratio of the size of the maximum effective regular workspace to the range of the actuated joints, we can see that the actuation efficiency is $2 \times l^* \approx 0.58$, which is relatively high. The values of ϑ and φ are both very close to $\pi/3$, which suggests that both the base and the moving platform degenerate to equilateral triangles and the corresponding joints coincide pairwise. In the optimal geometry, the size of the moving platform, b, tends to zero. This really reflects the requirement of workspace maximization.

Fig.19 shows distribution of the dexterity index $\kappa(\hat{J})$ at xy cross section of the resulting maximal effective regular workspace at $(z, \phi, \beta, \psi) = (z_c, 0, 0, 0)$. Fig.20-23 show distribution of the dexterity index at other four cross sections, where the minimal κ is equal to or very near $\gamma = 0.2$. Especially in Fig. 21 and 23, where respectively $z = z_c - l^*$ and $z = z_c + l^*$ while $(\phi, \beta, \psi) = (-20^o, 20^o, 20^o)$, $\kappa_{min} = 0.2000$. This indicates that the dexterity constraint (15) takes effect in those cases. Fig. 24 shows the cross sections of the workspace generated by the resulting manipulator at $z = z_c - l^*,\ z_c - l^*/2,\ z_c,\ z_c + l^*/2,\ z_c + l^*$ when $(\phi, \beta, \psi) = (0, 0, 0)$. The shadowed square, which is well contained in all five cross sections, is the corresponding cross section of the maximal effective regular workspace. Fig. 25 and 26 show two worst cases of workspace containment when $(\phi, \beta, \psi) = (20^o, -20^o, -20^o)$ and $(-20^o, -20^o, 20^o)$. In those cases, the maximal effective workspace touches the workspace boundary produced by the resulting manipulator.

VIII. DISCUSSIONS AND REMARKS

From the optimal results in the simulation, we can see that the sizes of moving platform are all very small, which indicates that a zero-size moving platform is desirable for the maximization of effective regular workspace. This coincides with the results by Gosselin and Angeles [8] for workspace maximization of a 3-RRR planar parallel manipulator. In the

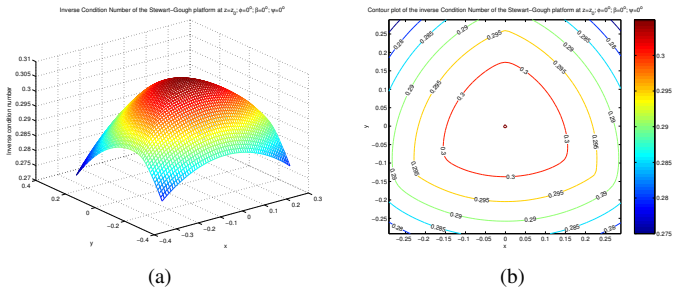

(a) (b)

Fig. 19. (a) Inverse condition number of $\hat{J}$ at $z = z_c$, and $(\phi, \beta, \psi) = (0, 0, 0)$; (b) Contour plot of the inverse condition number of $\hat{J}$ at $z = z_c$, and $(\phi, \beta, \psi) = (0, 0, 0)$.

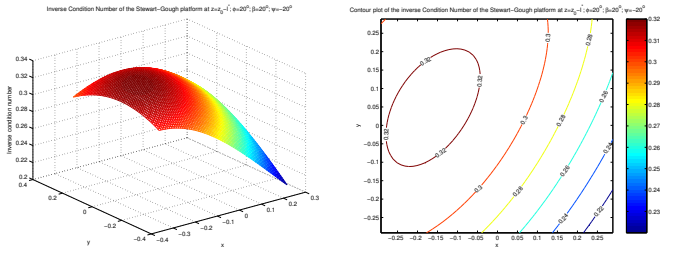

(a) (b)

Fig. 20. (a) Inverse condition number of $\hat{J}$ at $z = z_c - l^*$ and $(\phi, \beta, \psi) = (20^o, 20^o, -20^o)$; (b) Contour plot of the inverse condition number of $\hat{J}$ at $z = z_c - l^*$and $(\phi, \beta, \psi) = (20^o, 20^o, -20^o)$.

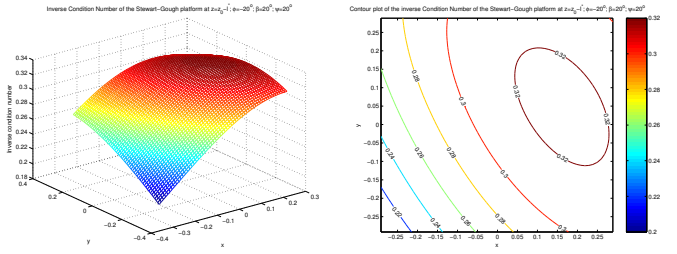

(a) (b)

Fig. 21. (a) Inverse condition number of $\hat{J}$ at $z = z_c - l^*$ and $(\phi, \beta, \psi) = (-20^o, 20^o, 20^o)$; (b) Contour plot of the inverse condition number of $\hat{J}$ at $z = z_c - l^*$and $(\phi, \beta, \psi) = (-20^o, 20^o, 20^o)$.

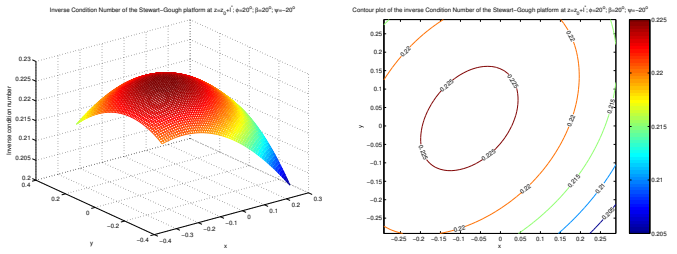

(a) (b)

Fig. 22. (a) Inverse condition number of $\hat{J}$ at $z = z_c + l^*$ and $(\phi, \beta, \psi) = (20^o, 20^o, -20^o)$; (b) Contour plot of the inverse condition number of $\hat{J}$ at $z = z_c + l^*$and $(\phi, \beta, \psi) = (20^o, 20^o, -20^o)$.

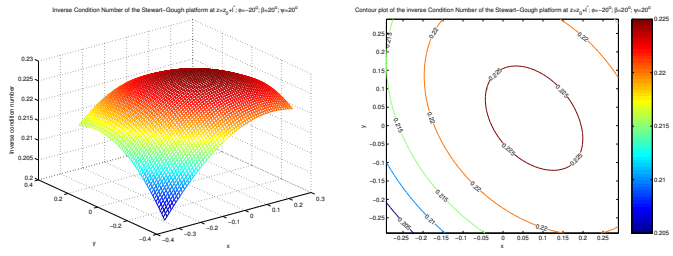

(a) (b)

Fig. 23. (a) Inverse condition number of $\hat{J}$ at $z = z_c + l^*$ and $(\phi, \beta, \psi) = (-20^o, 20^o, 20^o)$; (b) Contour plot of the inverse condition number of $\hat{J}$ at $z = z_c + l^*$and $(\phi, \beta, \psi) = (-20^o, 20^o, 20^o)$.

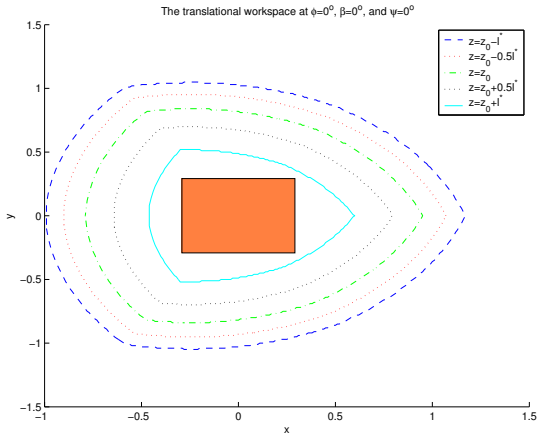

Fig. 24. xy workspace cross section at $z = z_c - l^*$, $z = z_c - l^*/2$, $z = z_c$,$z = z_c + l^*/2$, and $z = z_c + l^*$ when $(\phi, \beta, \psi) = (0, 0, 0)$

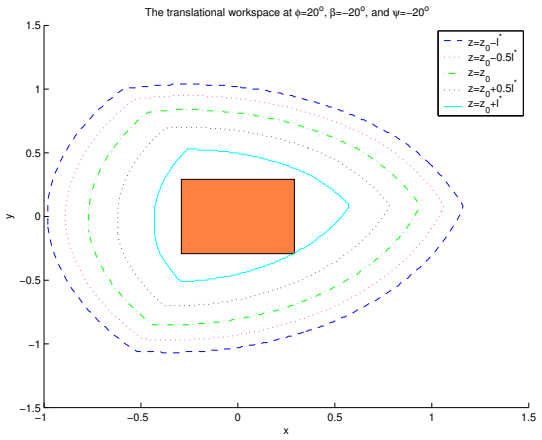

Fig. 25. xy workspace cross section at $z = z_c - l^*$, $z = z_c - l^*/2$, $z = z_c$,$z = z_c + l^*/2$, and $z = z_c + l^*$ when $(\phi, \beta, \psi) = (20^o, -20^o, -20^o)$

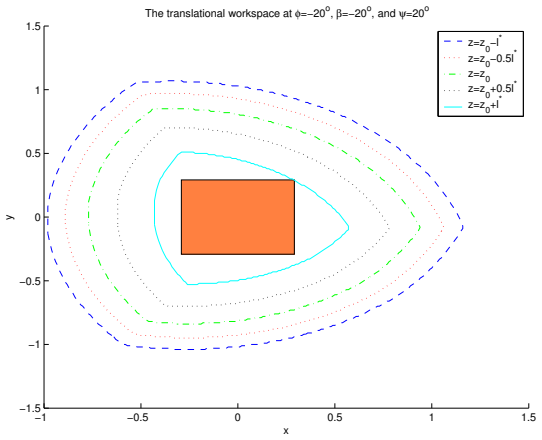

Fig. 26. xy workspace cross section at $z = z_c - l^*$, $z = z_c - l^*/2$, $z = z_c$,$z = z_c + l^*/2$, and $z = z_c + l^*$ when $(\phi, \beta, \psi) = (-20^o, -20^o, 20^o)$

example of the five-bar parallel linkage, the length of the base link is required to be zero.

In the examples of the five-bar parallel linkage, the 3-RRR planar parallel manipulator, and the DELTA robot, their minimal inverse condition number in the corresponding maximal effective regular workspace are all a little bit smaller than the prescribed one. In addition, the maximal effective regular workspaces of the optimal geometries of the five-bar parallel linkage and the DELTA robot exceed a little the workspace boundary generated by the corresponding optimal manipulators. Both constraints on workspace and inverse condition number are violated. This is simply because we discretize the Cartesian regular workspace and use the obtained nodes to represent constraints on all points over the regular workspace. This of course introduces errors. However, the errors are rather small and they're even acceptable in engineering design. On the other hand, we can reduce or eliminate the effects of discretization of regular workspace by applying a little bit stricter constraints of (15) and (16), say a little bit larger γ and a little bit smaller ranges for actuation.

In the simulation, the algorithm performed robustly. It converged regardless initial points. The simulation was conducted in the Matlab environment using a notebook computer with an Intel Pentium(M) processor of 1.3G. Also the running time is acceptable. Table VI shows some typical running times and independent variables of the previous design examples.

IX. Conclusion

In this paper, we presented a systematic procedure for kinematic synthesis of parallel manipulators. First, a novel and practical formulation for maximization of effective regular workspace was proposed. Then, we proposed a physically meaningful method for dealing with the dimensional inhomogeneity problem of the kinematic Jacobian. Finally, by the nature of the optimal design problem, the CRS technique was provided to solve the problem. It is reliable and robust. Kinematic synthesis of four typical parallel manipulators were carried out and the results show the effectiveness of the design procedure.

Example	1	1.1	2	3	4
No. ind. var.	3	6	3	3	5
running time (s)	140.1210	481.8330	267.5240	248.0370	14916

TABLE VI

Running time for simulations of different manipulators

APPENDIX I
CONVERGENCE PROOF BY SOLIS AND WETS

Solis and Wets [32] Considered a general minimization problem as follows.

Problem 6: Given a function $f : \mathbb{R}^p \to \mathbb{R}$ and a subset $S \subset \mathbb{R}^p$, find a point $\alpha \in S$ which minimizes f on S or at least which yields an acceptable approximation of the infimum of f on S.

They proposed a conceptual algorithm to solve the problem above. Clearly the CRS algorithm is in this category.

Algorithm *2:* The conceptual algorithm of Solis and Wets [32]

step 0: Find $\alpha^{(0)} \in S$ and set $k = 0$;

step 1: Generate $\xi^{(k)}$ from the sample space $(\mathbb{R}^p, \mathcal{B}, P_k)$, where $\mathcal{B}$ is the Borel σ-algebra on $\mathbb{R}^p$;

step 2: Set $\alpha^{(k+1)} = D(\alpha^{(k)}, \xi^{(k)})$, choose P_{k+1}, set $k = k + 1$ and return to step 2.

Here the map $D : S \times \mathbb{R}^p \to S$ satisfies the following condition.

(H1) $f(D(\alpha, \xi)) \leq f(\alpha)$ and if $\xi \in S$, $f(D(\alpha, \xi)) \leq f(\xi)$.

The P_k are probability measures corresponding to distribution functions of the k-th iteration defined on $\mathbb{R}^p$. The condition (H1) means that the map D can always produce a point $D(\alpha, \xi)$ which has a value of the objective function f no larger than the current minimum.

To exclude global minima that will be impossible to detect it is assumed that the global minimum of $f(\alpha)$ is the essential infimum f_e^* of $f(\alpha)$. The convergence to a point in the optimality region $R_{\epsilon,M}$ is considered where

$$R_{\epsilon,M} = \begin{cases} \{\alpha | \alpha \in S, f(\alpha) < f_e^* + \epsilon\}, & \text{if } f_e^* \text{ is finite} \\ \{\alpha | \alpha \in S, f(\alpha) < M\}, & \text{if } f_e^* = -\infty \end{cases}$$

and $\epsilon > 0$, $M < 0$.

(H2) *For any (Borel) subset A of S with $\nu(A) > 0$, we have that*

$$\prod_{k=0}^{\infty} [1 - P_k(A)] = 0,$$

where ν is a non-negative measure defined on the (Borel) subsets $\mathcal{B}$ of $\mathbb{R}^p$ with $\nu(S) > 0$. Typically $\nu(A)$ is simply the n-dimensional volume of the set A, more generally ν is the Lebesgue measure. It means that given any subset A of S with positive "volume", the probability of repeatedly missing the set A, when generating the random samples $\xi^{(k)}$, must be zero. This requires that the sampling strategy, which is determined by the choice of the P_k, cannot rely *exclusively* on distribution functions concentrated on proper subsets of S of lower dimension (such as discrete distributions) or that consistently ignore a part of S with positive "volume" with respect to ν.

Theorem *1:* Convergence Theorem

Suppose that f is a measurable function, S is a measurable subset of $\mathbb{R}^p$ and (H1) and (H2) are satisfied. Let $\{\alpha^{(k)}, k = 0, \cdots, \infty\}$ be a sequence generated by the algorithm. Then

$$\lim_{k \to \infty} P\{\alpha^{(k)} \in R_{\epsilon,M}\} = 1, \tag{34}$$

where $P\{\alpha^{(k)} \in R_{\epsilon,M}\}$ is the probability that at step k, the point $\alpha^{(k)}$ generated by the algorithm is in $R_{\epsilon,M}$.

Proof: From (H1) if follows that $\alpha^{(k)}$ or $\xi^{(k)}$ implies that $\alpha^{(l)} \in R_{\epsilon,M}$ for all $l \geq k + 1$. Thus

$$P\{\alpha^{(k)} \in R_{\epsilon,M}\} = 1 - P\{\alpha^{(k)} \in S - R_{\epsilon,M}\} \geq 1 - \prod_{i=0}^{k} (1 - P_i(R_{\epsilon,M}))$$

and hence

$$1 \geq \lim_{k \to \infty} P\{\alpha^{(k)} \in R_{\epsilon,M}\} \geq 1 - \lim_{k \to \infty} \prod_{i=0}^{k-1} (1 - P_i(R_{\epsilon,M})) = 1$$

where the last equality follows from (H2). This completes the proof.

REFERENCES

[1] J-P. Merlet. Designing a parallel manipulator for a specific workspace. *The International Journal of Robotics Research*, 16(4):545–556, 1997.

[2] J.-P. Merlet. An improved design algorithm based on interval analysis for spatial parallel manipulator with specified workspace. In *Proceedings of IEEE International Conference on Robotics and Automation*, pages 1289–1294, 2001.

[3] E. Ottaviano and M. Ceccarelli. Optimal design of CAPAMAN (Cassino parallel manipulator) with a specific orientation workspace. *Robotica*, 20(2):159–166, 2002.

[4] A. Kosinka, M. Galicki, and K. Kedzior. Designing and optimization of parameters of delta-4 parallel manipulator for a given workspace. *Journal of Robotic Systems*, 20(9):539–548, 2003.

[5] Y.J. Lou, G.F. Liu, J.J. Xu, and Z.X. Li. A general approach for optimal kinematic design of parallel manipulators. In *Proceedings of IEEE International Conference on Robotics and Automation*, pages 3659 – 3664, 2004.

[6] M. Guillot C.M. Gosselin. The synthesis of manipulators with prescribed workspace. *Transactions of the ASME, Journal of Mechanical Design*, 113(3):451–455, 1991.

[7] R.E. Stamper, L.W. Tsai, and G.C. Walsh. Optimization of a three dof translational platform for well-conditioned workspace. In *Proceedings of IEEE International Conference on Robotics and Automation*, pages 3250–3255, 1997.

[8] C. Gosselin and J. Angeles. The optimum kinematic design of a planar three-degree-of-freedom parallel manipulator. *ASME Journal of mechanisms, Transmissions, and Automation in Design*, 110, 1988.

[9] C. Gosselin and J. Angeles. The optimum kinematic design of a spherical three-dof-of-freedom parallel manipulator. *ASME Journal of mechanisms, Transmissions, and Automation in Design*, 111, 1989.

[10] H. H. Pham and I-M. Chen. Optimal synthesis for workspace and manipulability of parallel flexure mechanism. In *Proceeding of the 11th World Congress in Mechanism and Machine Science, Apr. 1-4, 2004,2004,edited by Tian Huang*, 2004.

[11] Michael Stock and Karol Miller. Optimal kinematic design of spatial parallel manipulators: Application of linear delta robot. *Transactions of the ASME, Journal of Mechanical Design*, 125(2):292–301, 2003.

[12] Dean C. Karnopp. Random search techniques for optimization problems. *Automatica*, 1(1):111–121, 1963.

[13] O. Khatib and A. Bowling. Optimization of the inertial and acceleration characteristics of manipulators. In *Proceedings of IEEE International Conference on Robotics and Automation*, pages 2883–2889, 1996.

[14] H. Lipkin and J. Duffy. Hybrid twist and wrench control for a robotic manipulator. *Transactions of ASME, Journal of Mechanisms, Transmissions, and Automation in Design*, 110(2):138–144, 1988.

[15] M. Tandirci, J. Angeles, and F. Ranjbaran. The characteristic point and characteristic length of robotic manipulator. In *Proc. ASME 22nd Biennial Conf. Robot., Spatial Mech. Mech. Syst.,* Scottsdale, AZ, Sept. 13-16, pages 203–208, 1992.

[16] O. Ma and J. Angeles. Optimum architecture design of platform manipulators. In *Proceedings of the Fifth International Conference on Advanced Robotics*, pages 1130 – 1135, 1991.

[17] J. Angeles. Kinematic isotropy in humans and machines. In *Proceedings of IFToMM 9th World Congress on Theory of Machines and Mechanisms*, pages XLII–XLIX, 1995.

[18] J. Angeles, F. Ranjbaran, and R.V. Patel. On the design of the kinematic structure of seven-axis redundant manipulators for maximum conditioning. In *Proceedings of IEEE International Conference on Robotics and Automation*, pages 494–499, 1992.

[19] L. Stocco, S. E. Salcudean, and F. Sassani. Fast constrained global minimax optimization of robot parameters. *Robotica*, 16(6):595–605, 1998.

[20] L. Stocco, S. E. Salcudean, and F. Sassani. On the use of scaling matrces for task-specific robot design. *IEEE Transactions on Robotics and Automation*, 15(5):958–965, 1999.

[21] O. Ma and J. Angeles. Architecture singularities of platform manipulators. In *Proceedings of IEEE International Conference on Robotics and Automation*, pages 1542–1547, 1991.

[22] J.A. Snyman and A.M. Hay. The dynamic-q optimization method: An alternative to SQP? *Computers and Mathematics with applications*, 44(12):1589–1598, 2002.

[23] G.V. Reklaitis, A. Ravindran, and K.M. Ragsdell. *Engineering Optimization: Methods and Applications*. John Wiley and Sons, 1st edition, 1983.

[24] A. Törn and A. Žilinskas. *Global Optimization*. Springer-Verlad, 1st edition, 1989.

[25] R.L. Anderson. Recent advances in finding best operating conditions. *Journal of the American Statistical Association*, 48(264):789–798, 1953.

[26] S.H. Brooks. A discussion of random methods for seeking maxima. *Operations research*, 6(2):244–251, 1958.

[27] L.A. Rastrigin. The convergence of the random search method in the extremal control of a many-parameter system. *Automation and Remote Control*, 24:1337–1342, 1963.

[28] M.A. Schumer and K. Steiglitz. Adaptive step size random search. *IEEE Transactions on Automatic Control*, 13(3):270–276, 1968.

[29] R. Luus and T.H.I. Jaakola. Optimization by direct search and systematic reduction of the size of search region. *AIChE Journal*, 19(4):760–766, 1973.

[30] T.W. Lee and F. Freudenstein. Heuristic combinatorial optimization in the kinematic design of mechanisms, part 1: theory. *Transactions of ASME, Journal of Engineering for Industry*, pages 1277–1280, 1976.

[31] Luc P. Devroye. Progressive global random search of continuous functions. *Mathematical programming*, 15:330–342, 1978.

[32] Francisco J. Solis and Roger J-B. Wets. Minimization by random search techniques. *Mathematics of operations research*, 6(1):19–30, 1981.

[33] R.L. Salcedo. Solving nonconvex nonlinear programming and mixed-integer nonlinear programming problems with adaptive random search. *Industrial and Engineering Chemistry Research*, 31(1):262–273, 1992.

[34] R.L. Salcedo, M.J. Gonçalves, and S. Feyo de Azevedo. An improved random-search algorithm for non-linear optimization. *Computers and Chemical Engineering*, 14(10):1111–1126, 1990.

[35] saul B. Gelfand and Sanjoy K. Mitter. Recursive stochastic algorithms for global optimization in $\mathbb{R}^d$. *SIAM journal on control and optimization*, 29(5):999–1018, 1991.

[36] J.R. Banga and W.D. Seider. Global optimization of chemical processes using stochastic algorithms. *State of the Art in Global Optimization: Computational Methods and Applications, C.A. Floudas and P. M. Pardalos (Eds.), Kluwer Academic Publishers*, pages 563–583, 1996.

[37] P.P. Khargonekar and A. Yoon. Random search based optimization algorithms in control analysis and design. In *Proceedings of the American Control Conference*, pages 383–387, 1999.

[38] J.-Q. Lu and T. Adachi. A semi-random searching algorithm for global optimization design on electronic circuits. In *Proceedings of the IEEE International Sympoisum on Circuits and Systems*, pages 1697 – 1700, 1991.

[39] D.I. Olcan. Adaptive random search for antenna optimization. In *Proceedings of the Antennas and Propagation Society Symposium*, pages 1114–1117, 2004.

[40] R. Goulcher and J.J. Casares Long. The solution of steady-state chemical engineering optimisation problems using a random search algorithm. *Computers and Chemical Engineering*, 2(1):33–36, 1978.

[41] M.W. Heuckroth, J.L. Gaddy, and L.D. Gaines. An examination of the adaptive random search technique. *AIChE Journal*, 22(4):744–750, 1976.

[42] J.P. Karidis, G. McVicker, J.P. Pawletko, L.C. Zai, M. Goldowsky, R.E. Brown, and R.R. Comulada. The hummingbird minipositioner-providing three-axis motion at 50 g's with low reactions. In *Proceedings of IEEE International Conference on Robotics and Automation*, pages 685–692, 1992.

[43] V. Hayward, J. Choksi, G. Lanvin, and C. Ramstein. Design and multi-objective optimization of a linkage for a haptic interface. In *Advances in robot kinematics and computational geometry, J. Lenarčič and B. Ravani editors*, pages 352–359, 1994.

[44] R. Clavel. Delta, a fast robot with parallel geometry. In *Proc. 18th International Symposium on Industrial Robots*, pages 91–100, 1988.

[45] F. Sternheim. Tridimensional computer simulation of a parallel robot. Results for the 'DELTA4' Machine. In *Proc. 18th International Symposium on Industrial Robots*, pages 333–340, 1988.

PLACE PHOTO HERE

Yunjiang Lou Biography text here.

PLACE PHOTO HERE

Guanfeng Liu Biography text here.

PLACE PHOTO HERE

Zexiang Li Biography text here.